ELSEVIER

International Journal of Applied Earth Observation and Geoinformation 4 (2003) 217–229

INTERNATIONAL JOURNAL OF APPLIED EARTH OBSERVATION AND GEOINFORMATION

www.elsevier.com/locate/jag

A segmentation and classification approach of IKONOS-2 imagery for land cover mapping to assist flood risk and flood damage assessment

C.J. van der Sande [a,1], S.M. de Jong [b,*], A.P.J. de Roo [c,2]

[a] *Netherlands Geomatics and Earth Observation BV, Postbus 2176, 3800 CD Amersfoort, The Netherlands*
[b] *Faculty of Geographical Sciences, Utrecht University, P.O. Box 80.115, 3508 TC Utrecht, The Netherlands*
[c] *European Commission, Joint Research Centre, Institute of Environment and Sustainability, Natural Hazards Project—Floods, LM Unit Via E. Fermi, TP 261, 21020 Ispra (Va), Italy*

Received 31 July 2002; accepted 31 January 2003

Abstract

Various regions in Europe have suffered from severe flooding over the last decennium. Earth observation techniques can contribute toward more accurate flood hazard modelling and they can be used to assess damage to residential properties, infrastructure and agricultural crops. For this study, detailed land cover maps were created by using IKONOS-2 high spatial resolution satellite imagery. The IKONOS-2 image was first divided into segments and the land cover was classified by using spectral, spatial and contextual information with an overall classification accuracy of 74%. In spite of the high spatial resolution of the image, classes such as residential areas and roads are still fairly difficult to identify. The IKONOS-2-derived land cover map was used as input for the flood simulation model LISFLOOD-FP to produce a Manning roughness factor map of inundated areas. This map provides a more accurate spatial distribution of Manning's roughness factor than maps derived from land cover datasets such as the EU CORINE land cover dataset. CORINE-derived roughness maps provide only averaged, lumped values of roughness factors for each mapping unit and are hence less accurate. Next, a method to produce a property damage map after flooding is presented. The detailed land cover map, water depth estimates resulting from the LISFLOOD-FP model, and known relations between water depth and property damage yielded a map of estimated property damage for the 1995 flood which affected the villages of Itteren and Borgharen in the southern part of The Netherlands. Such a map is useful information for decision makers and insurance companies.

Keywords: Image segmentation; LISFLOOD flood simulation; Stage-damage curve; IKONOS-2 image

1. Introduction

Over the last 10 years dramatic river flooding has affected various regions all over the world. Examples of such massive floods are the Meuse (The Netherlands in 1993), the Rhine and the Meuse (The Netherlands, Belgium and Germany in 1995 and 1996), the Oder (Czech Republic, Poland and Germany in 1997),

* Corresponding author. Tel.: +31-30-253-2749/4050; fax: +31-30-253-1145.
E-mail addresses: cvandersande@yahoo.com (C.J. van der Sande), s.dejong@geog.uu.nl (S.M. de Jong), ad.de-roo@jrc.it (A.P.J. de Roo).
[1] Tel.: +33-463-7433; fax: +33-463-7340.
[2] Tel.: +39-0332-786240; fax: +39-0332-785500.

0303-2434/03/$ – see front matter © 2003 Elsevier Science B.V. All rights reserved.
doi:10.1016/S0303-2434(03)00003-5

the Tisza (Hungary and Rumania in 2000), various rivers in Yorkshire and Midlands (UK in 2000), the Po (Italy in 2000), the Elbe and Styre (Germany and Austria in 2002) and the Gard (France in 2002). Hydrologic flood modelling at the spatial scale of a river basin is a useful tool to understand the causes of flood events. Different kinds of models to simulate flooding and runoff have been developed in the past decades. An important parameter in these models is the (Manning) roughness coefficient which comprises a flow resistant factor and a function of land cover in flooded areas (De Roo, 1999; De Roo et al., 1999a). This specific factor is difficult to determine because detailed and actual land cover information is usually not available. Furthermore, for the assessment of property damage caused by a flood, a flood extent map and a flood depth map must be combined with a detailed land cover map. Early property damage assessment and accurate modelling of flood events require that private-owned objects, agricultural land use and infrastructure are identified on a land cover map.

The areas most vulnerable to damage by flooding are urban landscapes. Urban landscapes are composed of varied materials (concrete, asphalt, metal, plastic, glass, shingles, water, grass, shrubs, trees, and soil) arranged by humans in complex ways for the construction of houses, transportation systems, utilities, commercial buildings, gardens, parks, playgrounds and other recreational landscapes. Land cover maps are readily available in different classification systems and scales throughout the world but seldom at the required spatial detail. Another constraint is that these land cover maps are not interchangeable, while flood events very often occur at transnational level. A good and promising alternative is to derive land cover maps from earth observation images. Images are collected at various spatial resolutions and are frequently available. With the launch of IKONOS-2 in September 1999, one-meter resolution panchromatic and four-meter multi-spectral images became available. Image analysis at this spatial resolution enables the identification of urban and sub-urban objects. A spatial resolution of 0.25 m to maximum 5 m is generally thought to be sufficient to detect or distinguish types of buildings and individual buildings (Jensen and Cowen, 1999). IKONOS-2 fulfils these requirements. In practice however, it proves difficult to classify these high-resolution images on a pixel-by-pixel basis due to the high level of information captured by these images (Blaschke and Strobl, 2002; Hofmann, 2001; Limp, 2002; De Jong et al., 2000). Important semantic/spatial information required to interpret the image is not accounted by the pixel-by-pixel classification algorithms. In the past two decades various segmentation techniques have been developed to incorporate context, or neighborhood information, in the image classification procedure e.g. Roberts, 1970; Ballard and Brown, 1982; Tilton, 1989 and Janssen, 1994. Most of these methods are experimental or developed for research experiments only (Schoenmakers, 1995; Wilson and Spann, 1988). The new software package eCognition (eCognition, 2002) brings together several of these contextual and object-oriented approaches and gives promising results for high-resolution image analysis. The new method used in this study first extracts image objects by segmentation. The segments are subsequently classified using combinations of spectral and spatial information (Baatz and Schäpe, 2000). The objective of this study is to investigate the usefulness of high spatial resolution IKONOS-2 imagery and segmentation algorithms to produce detailed land cover maps for flood damage assessment as well as detailed maps of roughness coefficients for flood simulation models.

2. Study area

The study site selected is located in southern part of The Netherlands around the villages of Itteren and Borgharen and approximately 10 km north of the city of Maastricht as shown in Fig. 1. The area measures approximately 16 km^2 and comprises agricultural land, residential areas and a few industrial sites. East of the flood plain of the river is a canal (the Julianakanaal) which was constructed to allow ships to bypass shallow parts of the river. The two villages of Itteren and Borgharen are located in the flood plain of the river. In January 1995 severe flooding of the Meuse inundated the entire area between the Meuse and the canal and wreaked significant damage on the two villages and the agricultural activities (Fig. 1). Details about financial or local economic losses are not available for this flood except that the total financial damage including evacuation costs for The

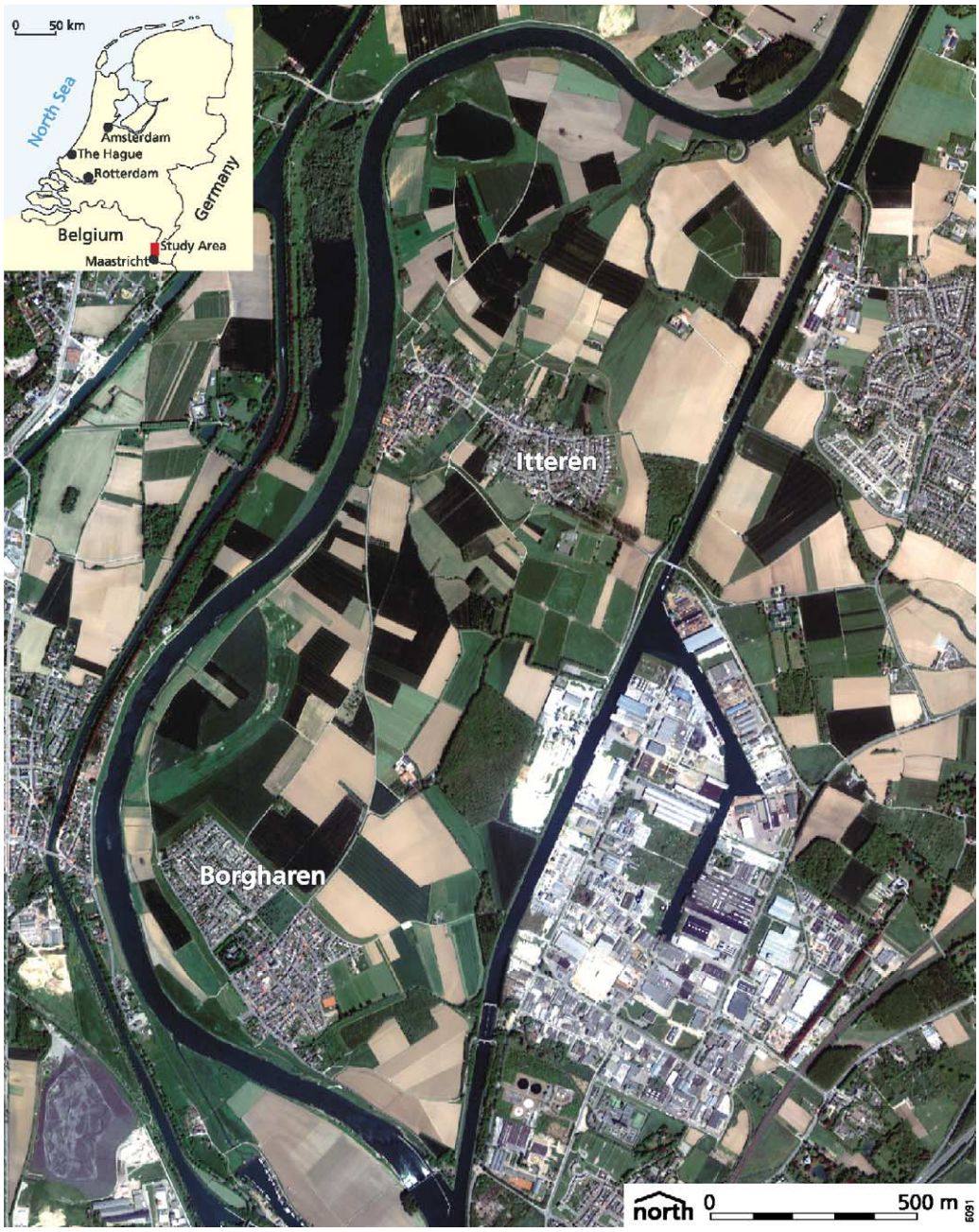

Fig. 1. Location of the study area (left) and the area as registered by IKONOS-2 (right).

Netherlands and Belgium was estimated at € 3.5 billion. In The Netherlands individuals and enterprises are generally not insured against water damage due to flooding.

3. Image analysis

The image used in this study for detailed land cover mapping is a ‘pan-sharpened’ multi-spectral

IKONOS-2 image acquired on 6 May 2000. A subset image was created and centred over the villages of Itteren and Borgharen. Table 1 provides detailed characteristics of the IKONOS-2 image used in this study.

A land use classification scheme was designed for the study area and appropriate for the IKONOS-2 image. The basis for this scheme was adapted from the land use classification system of the 'United States Geological Service (USGS) land use and land cover classification system for use with remotely sensed data' proposed by Anderson et al. (1976). This system is designed to use four levels of information, levels I and II are specified by the USGS. The user specifies levels III and IV, keeping in mind that the categories in each level must aggregate into the categories in the next higher level. The category in level III was created for satellite data having a resolution ranging from 1 to 5 m. Level III is the appropriate level of scale for the IKONOS-2 image. Level IV is the category for remotely sensed imagery with a resolution of 0.3–1.0 m i.e. aerial photography. Table 2 provides an overview of the land cover classes and the different level of scales as applied to this study.

Image classification is the process of assigning individual pixels or groups of pixels to thematic classes (Richards, 1999). Supervised classification requires

Table 1
Image specifications of the IKONOS-2 image of Itteren and Borgharen

Image specifications	
Acquisition date and time	6 May 2000 at 10.31 a.m.
Spatial resolution	1 m panchromatic sharpened multi-spectral bands
Spectral wavebands	0.45–0.53 μm (blue), 0.52–0.61 μm (green), 0.64–0.72 μm (red), 0.77–0.88 μm (near IR)
Data format	2048 grey levels (11 bits)
Solar elevation angle	53.8°
Solar azimuth angle	154.1°
Map projection	Universal transverse mercator
Nominal azimuth collection	248.8°
Nominal elevation collection	80.1°
Processing level	Standard geometrically corrected
General information	
Ground track revisit time	11 days
Revisit time for imaging	3.2 days at 1 m resolution; 1 day at 2 m resolution
Altitude	682 km sun-synchronous orbit
Inclination angle	98.1°
Orbit time	98 min
View angle	Nadir
Swath width	11 km

Table 2
Land use classification system for the IKONOS-2 image

Level I	Level II	Level III
(1) Urban/built-up land	(11) Residential	(111) Residential building
		(112) Private/public garden
		(113) Grass in built-up area
		(114) Pavement/other urban area
		(115) Water side
	(13) Industry	(131) Sand deposit area
	(14) Transportation, communications, and utilities	(141) Road
		(143) Railroad
	(15) Industrial and commercial complexes	(151) Industrial company
(2) Agricultural land	(21) Cropland and pasture	(211) Pasture
		(212) Winter wheat
	(22) Orchard, groves, vineyards, nurseries, and horticultural areas	(221) Nursery
	(24) Other agricultural land	(241) Fallow
(3) Rangeland	(33) Mixed rangeland	(331) Natural vegetation
(4) Forest land	(41) Deciduous forest land	
	(42) Mixed forest land	
(5) Water		

'ground truth' data from any source to direct the classification process. The essential five steps of a supervised image classification are: (1) decide on the ground cover types to be classified such as water, urban areas, agricultural croplands, etc.; (2) choose prototype pixels with known land cover to form training data on the basis of site visits, maps and aerial photographs; (3) define the set of parameters of that class i.e. the spectral signature and/or the spatial characteristics; (4) classify every pixel in the image using a user-defined classification algorithm; and (5) evaluate the obtained accuracy. As the traditional per-pixel classification methods are not very suited for the new higher-resolution data due to their large, detailed information content (Blaschke and Strobl, 2002; Hofmann, 2001; Limp, 2002; De Jong et al., 2000) we decided to use an image classification approach that does not only account for spectral information but also for local patterns in the image by a group of neighboring pixels. The segmentation techniques developed over the past decades can broadly be divided into three categories (Ballard and Brown, 1982): (1) edge-finding (Roberts, 1970); (2) region-growing (Tilton, 1989); and (3) map or knowledge-based segmentation (Janssen, 1994). The method used here is an advanced region-growing and knwoledge-based segmentation approach. The algorithms are based on the conceptual idea that important semantic information required to interpret an image is not represented in single pixels but in meaningful image objects and their mutual relations, i.e. the context. The segmentation algorithm is a bottom-up region-growing technique starting with one-pixel objects. In many subsequent steps smaller image objects are merged into larger ones (more pixels). The growing decision is based on local homogeneity criteria describing the similarity of adjacent image objects in terms of size, distance, texture, spectral similarity and form (Baatz and Schäpe, 2000). User-defined thresholds are interactively used to decide whether objects are merged into larger objects or not (eCognition, 2002). The procedure of growing stops when merges obeying the user's criteria are no longer possible. The first step in the image analysis was to generate homogeneous objects or segments on the basis of the four spectral bands and contextual information. Four levels of segmentation steps proved to give the optimal classification results. At each level it is possible to extract specific thematic classes from the image.

Table 3 shows the segmentation parameters used as relative values and as a function of thematic land cover. As shown in Table 3 the spectral bands can either be included or excluded from the segmentation process as a function of their information content. The scale parameter was the most important factor to control the size of the objects. Color and shape were weighted according to the type of thematic land use. The settings of the shape parameter appeared to provide pertinent information with respect to the land cover and were therefore assigned a high impact value. Segmentation at level IV was used to classify the larger objects in the study area such as agricultural fields and water bodies. The red and near-infrared spectral bands were used together with the homogeneity criterion for the classification of vegetation types, crops as well as water bodies (Table 3). Small roads were extracted from segmentation at level III using the green, red and near-infrared spectral bands and the homogeneity and shape criteria. Buildings were extracted from level II, where a scale parameter of 10 resulted in objects small enough to differentiate individual houses. In the next step of the image analysis the various

Table 3
Segmentation parameters used for the analysis of the IKONOS-2 image

Segmentation and classification level	Land use types	IKONOS bands used				Scale	Homogeneity criterion			
		Blue	Green	Red	NIR		Color	Shape	Shape settings	
									Smoothness	Compactness
Level I	All	Yes	Yes	Yes	Yes	5	0.7	0.3	0.9	0.1
Level II	Buildings	No	Yes	Yes	Yes	10	0.5	0.5	0.9	0.1
Level III	Roads	No	Yes	Yes	Yes	30	0.5	0.5	0.9	0.1
Level IV	Agriculture, water, large buildings and roads	No	No	Yes	Yes	100	0.9	0.1	0.9	0.1

segmentation levels are classified using 'ground truth' information on the basis of the land cover scheme presented in Table 2. Ground truth information was collected from field visits, topographical maps and aerial photographs. The strength of the new object-oriented approach is that apart from spectral features, it also uses local spatial features such as surface area, length and width of objects during the classification process. Moreover, the ability to use relations between neighboring objects and relations between objects classified at different levels with finer or courser segments was useful during image classification.

Vegetation cover is classified in level IV. Deciduous forest is classified using spectral information and object-related properties. Deciduous forest is quite heterogeneous compared to other vegetation classes like winter wheat or meadows due to shade and gaps in the forest canopy. This heterogeneity is accounted for by the high standard deviation in the near-infrared spectral band. In the study area several tree nurseries are found and these nurseries have similar spectral characteristics as a deciduous forest. However, the spatial arrangement of trees in a nursery is different because the trees are planted in straight rows. These rows of trees were identified by a ratio of length and width of the object and could easily be distinguished. Roads were also classified using the length/width information in level III and IV. Houses are related to black segments i.e. shadow in the image. All objects with spectral values of a house and their position next to a dark shadow object are accordingly correctly classified as a house. After careful evaluation of the various intermediate results the classification results per level are merged into level I and exported as a thematic land cover layer. In the next section of this article the obtained accuracy of the land cover classification, the methods to assess flood damage using the IKONOS-2-derived land cover map and roughness parameters are presented and discussed.

4. Results

4.1. Land cover map

The land cover map of the study area resulting from the object-oriented image classification approach is presented in Fig. 2. It is impressive to see the amount of detail concerning agricultural crops and residential areas captured in this image acquired at an altitude of 682 km. Individual buildings and parcel boundaries can easily be identified. The error matrix of the image classification was computed to determine the accuracy of the land cover map. The error matrix is based on 565 sample points and shown in Table 4. The overall accuracy of the classification is 74%. The KHAT statistic, a measure of the difference between the actual agreement between reference data and an automated classifier and the chance agreement between the reference data and a random classifier (Lillesand and Kiefer, 2000), is 0.70. Results are quite good as might be expected with this detailed imagery. The accuracy for pasture, winter wheat, fallow and water are very good, over 95% correctly classified. Some poorly identified classes are gardens, grass within built-up areas, riverbanks, some roads, industrial areas and sand deposit areas. Classification confusion occurs between pasture and natural vegetation, roads and other pavements and roads and residential buildings.

Comparing the total built-up surface area determined from the topographical map (1:25,000) and the area classified in the IKONOS-2 image provided an alternative assessment of the accuracy of the classification which turned out to be very good. The total built-up surface area computed from the topographical map is 45,996 m^2 and from the image 42,539 m^2. The built-up area derived from the topographical map was overlaid with the built-up area extracted from the IKONOS-2 image and yielded information about the positional accuracy. Fig. 3 presents these two built-up areas side by side. Visual inspection and overlaying revealed that the shape of the buildings is sometimes different and that there are some small positional errors. The buildings on the IKONOS-2 image show irregular forms probably caused by blurring of the spectral information of the image. At this moment it is hard to determine the effects of the various sources of errors such as geometric precision, absent buildings on the topographical map and erroneous classifications on the further analyses.

4.2. Improved flood risk assessment

Assessing flood risk can be achieved by using high-resolution flood inundation simulations, such as the flood plain (FP) modules available in the

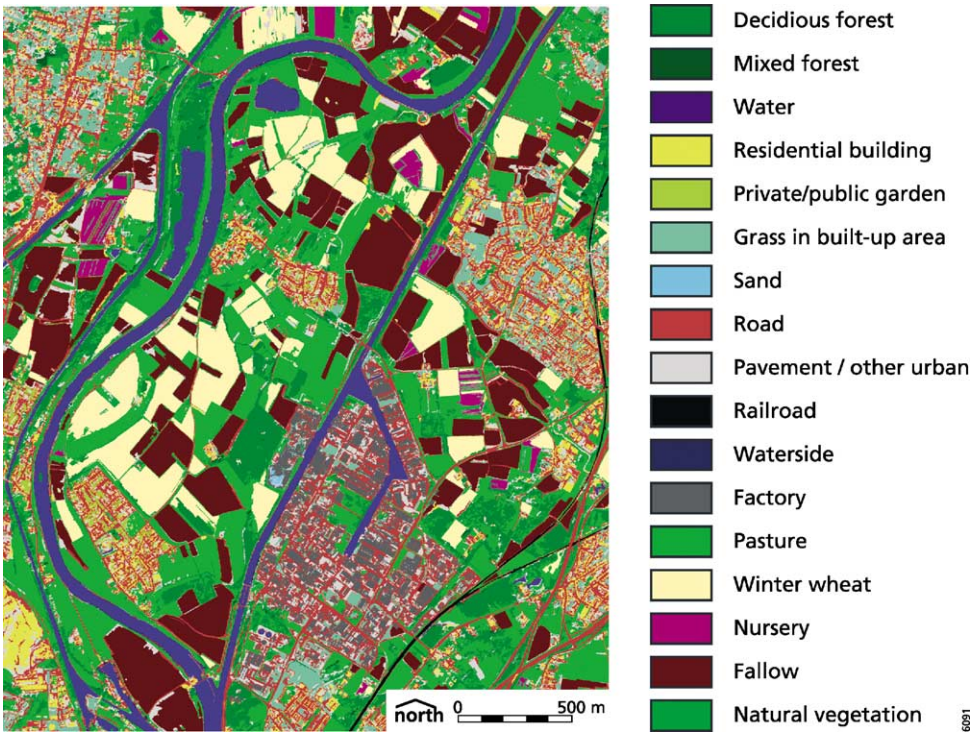

Fig. 2. IKONOS-2-derived land cover map for the Borgharen study area.

LISFLOOD model: LISFLOOD-FP (Bates and De Roo, 2000; De Roo et al., 2000). LISFLOOD-FP is a high-resolution flood inundation model whose aim/objective is to simulate accurate flood extent and flood depth maps. The main inputs in the LISFLOOD flood plain model are a high-resolution Digital Elevation Model (DEM): 25 or 50 m horizontal grid or better and a 10–20 cm vertical accuracy, an inflow hydrograph, river geometry and a floodplain friction factor such as the earlier-mentioned Manning's roughness factor n. The hypothesis tested here is whether a more detailed floodplain friction map, derived from the IKONOS-2 land cover map, would improve flood risk estimations, as compared to the use of friction maps obtained from a coarser, EU CORINE land use map. The LISFLOOD-FP simulation model was used to produce a maximum flood extent map for the Meuse flood of January 1995 in the study area surrounding the villages of Itteren and Borgharen. A flood extent map from an air photo was available to validate the model simulations as presented in Fig. 4. A flood extent map derived from an ERS-SAR microwave image (De Roo et al., 1999b) was also used to compare model simulations. The extent of agreement between the ERS-SAR flood extent map and the model simulations agree is approximately 85%.

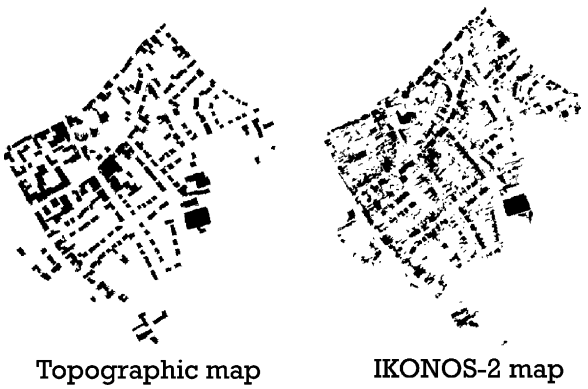

Fig. 3. Comparison of buildings, in black, extracted from the topographical map 1:25,000 and as classified in the IKONOS-2 image land cover classification in the southern part of the village of Borgharen (see Fig. 1).

Table 4
Error matrix of the IKONOS-2 land cover classification

IKONOS classification	Ground truths																		Users' sum accuracy		Class-map accuracy
		111	112	113	114	115	141	143	132	151	211	212	221	241	331	41	43	5			
Residential building	111	18	0	0	3	0	3	0	0	0	0	2	0	0	0	0	0	0	26	0.69	0.44
Garden	112	0	10	0	0	0	0	0	0	0	0	0	0	0	1	0	0	0	11	0.91	0.56
Grass in built-up area	113	0	1	12	1	0	1	0	0	0	0	0	0	0	0	1	0	0	16	0.75	0.63
Pavement/other urban	114	4	1	0	39	0	1	0	1	7	0	0	0	1	2	2	0	0	58	0.67	0.57
Waterside	115	0	0	0	0	1	0	0	0	0	0	0	0	1	0	0	0	0	2	0.50	0.25
Road	141	11	0	2	23	1	36	0	1	3	0	0	0	1	4	0	0	0	82	0.44	0.41
Railroad	143	0	0	0	0	0	0	4	0	0	0	0	0	0	0	0	0	0	4	1.00	1.00
Sand deposit area	132	0	0	0	0	0	0	0	7	0	0	0	0	0	0	0	0	0	7	1.00	0.50
Industrial company	151	0	0	0	10	0	0	0	5	17	0	0	0	0	0	0	0	0	32	0.53	0.40
Pasture	211	0	5	1	2	0	0	0	0	0	123	0	1	1	22	8	0	0	163	0.75	0.74
Winter wheat	212	0	0	0	0	0	0	0	0	0	1	37	0	0	0	0	0	0	38	0.97	0.80
Nursery	221	0	0	0	0	0	0	0	0	0	0	0	5	0	0	0	0	0	5	1.00	0.83
Fallow	241	0	0	0	0	0	0	0	0	0	1	0	0	42	0	0	0	0	43	0.98	0.89
Natural vegetation	331	0	0	0	0	0	0	0	0	0	0	3	0	0	4	0	0	0	7	0.57	0.10
Deciduous forest	41	0	0	0	0	1	0	0	0	0	2	3	0	0	3	23	1	0	33	0.70	0.52
Mixed forest	43	0	0	0	0	0	0	0	0	0	0	0	0	0	0	0	6	0	6	1.00	0.86
Water	5	0	0	0	0	0	0	0	0	0	0	0	0	0	0	0	0	32	32	1.00	1.00
Sum		33	17	15	78	3	41	4	14	27	127	45	6	46	36	34	7	32	565		
Producers' accuracy		0.55	0.59	0.80	0.50	0.33	0.88	1.00	0.5	0.63	0.97	0.82	0.83	0.91	0.11	0.68	0.86	1.00			
Overall accuracy		0.74																			
KHAT accuracy		0.70																			

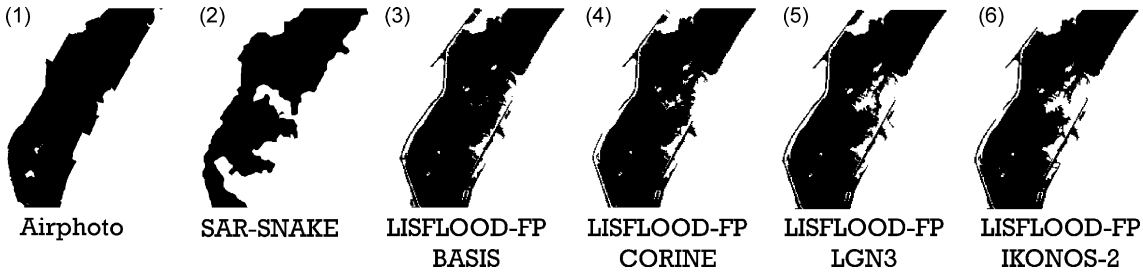

Fig. 4. Flood extent maps derived from various sources for the Borgharen study site shown in Fig. 1. Black indicates inundated areas. From left to right: flood extent mapped from (1) an aerial photo; (2) from an ERS-SAR microwave image. Flood extent modelled by the LISFLOOD-FP model (De Roo et al., 1999b) using (3) one Manning's *n* value for the entire flood plain; (4) Manning's *n* derived from the EU CORINE land cover data; (5) Manning's *n* derived from the Dutch LGN-3 land cover data and (6) Manning's *n* derived from IKONOS-2 land cover map.

The characteristics of the DEM and the friction in the flood plain (Manning roughness coefficient) control the flood extent on the flood plain during the simulations. Fixed Manning roughness coefficients (value of 0.060) would normally be assigned to each land cover class (Bates and De Roo, 2000). Coarser land use maps used for model runs are the European CORINE land cover map with a 100 m resolution and the Dutch LGN-3 (Thunnissen and De Wit, 2000) land cover map with a 25 m resolution. Here, the use of IKONOS-2 to produce a more detailed Manning floodplain friction map on the basis of derived land cover is investigated and compared with other simulations. Manning's values used for specific land cover are listed in Table 5. The flood extent map created with the IKONOS-2-derived Manning information was compared with the flood extent map created with a fixed Manning coefficient. Moreover, the LISFLOOD model runs were compared to investigate whether the adjusted Manning coefficient resulted in other simulated values of discharge and water depth.

Changing the floodplain Manning coefficient resulted in significant differences of the flood simulations. Table 6 shows the computed accuracy values of the different flood extent maps compared with an airphoto interpretation map as ground truth. The accuracy of the derived flood extent maps is high, but it should be noted that when only two classes (flooded, non-flooded) are used, the probability of obtaining good classification results just by chance is high. As a result, the KHAT values are quite modest in spite of the good values of overall accuracy. As discussed in Bates and De Roo (2000) the LISFLOOD model with a lumped Manning coefficient performs rather satisfactorily. The spatial adjustments to the Manning coefficient by using the land use maps of CORINE, LGN-3 (Thunnissen and De Wit, 2000) and the map derived from IKONOS-2 show varying results. Fig. 4 shows the different flood extent maps. The hydrograph and

Table 5
Manning roughness coefficients

Land use classes	Manning roughness coefficient	Source
(111) Residential building	0.200	
(112) Private/public garden	0.100	Chow (1959)
(113) Grass in built-up area	0.259	De Roo (1999)
(114) Pavement/other urban area	0.050	
(115) Waterside	0.050	
(131) Sand deposit area	0.120	De Roo (1999)
(141) Road	0.013	Chow (1959)
(143) Railroad	0.033	Chow (1959)
(151) Industrial company/agency	0.200	Chow (1959)
(211) Pasture	0.259	De Roo (1999)
(212) Winter wheat	0.127	De Roo (1999)
(221) Nursery	0.200	Beasley and Huggins (1982)
(241) Fallow	0.120	De Roo (1999)
(331) Natural vegetation	0.100	Chow (1959)
(41) Deciduous forest land	0.200	Beasley and Huggins (1982)
(43) Mixed forest land	0.200	Beasley and Huggins (1982)
(5) Water	0.030	Chow (1959)

Table 6
Accuracy values flood extent maps

	SAR-snake	LISFLOOD-basis	LISFLOOD-corine	LISFLOOD-lgn	LISFLOOD-Ikonos
Producers' accuracy	0.83	0.98	0.96	0.93	0.92
Users' accuracy	0.91	0.91	0.93	0.91	0.92
Map accuracy (water)	0.77	0.89	0.89	0.85	0.85
Map accuracy (not water)	0.55	0.61	0.62	0.54	0.55
Overall accuracy	0.82	0.91	0.91	0.87	0.87
KHAT accuracy	0.58	0.70	0.71	0.62	0.63

water depth of the outlet of the river channel showed that the rising and falling limbs of the four simulations were approximately the same.

The conclusion of these simulations is that the flood extent map produced by using the IKONOS-2 image to obtain a floodplain friction map differs from the other simulations only at a limited number of locations. Based on the sparsely available reference data it is difficult to judge which simulation is better. It seems that in this case the extremely large amount of water on the floodplain is the dominant factor for the flood extent and not the local friction produced by objects. A more detailed input map on floodplain friction derived from IKONOS-2 will produce better spatial maps of flood development (flow direction, water depth) over the floodplain for less extreme events which is useful information to understand the flooding process.

4.3. Flood damage assessment

Flood damage assessment methods which were developed since 1945 (White, 1945) were initiated by governments and insurance companies. The methods vary from fairly simple relationships between water depth and estimated financial damage to rather complex models requiring data on flood velocity, water depth, building characteristics, cost of repair, people's behavior and estimates of indirect economic losses (Penning-Rowsell and Fordham, 1994; HAZUS, 2001). The economic value of the land use type must be known in order to calculate the real financial damage. This value is normally based on the principle of replacement value: what are the costs of replacing a similar object? In this study, the land cover information extracted from the IKONOS-2 image was used in combination with water depth and the values of estimated costs obtained from the literature to assess the damage costs for the 1995 flood event. Water depth-damage curves for each land cover class were collected from the literature (Vrisou van Eck and Kok, 2001; Kok, 2001; Penning-Rowsell, 2001; Staatscourant, 1998) and summarized in Fig. 5 and Table 7.

The total estimated damage for the study area was calculated by using combined information from the flood extent map, the water depth during flooding produced by the LISFLOOD simulation model, the IKONOS-2-derived land cover map and the depth-damage curves from the literature. The following assumptions were made to execute the flood damage assessment:

- Damage functions are related only to water depth, although flood damage is controlled by various other variables.

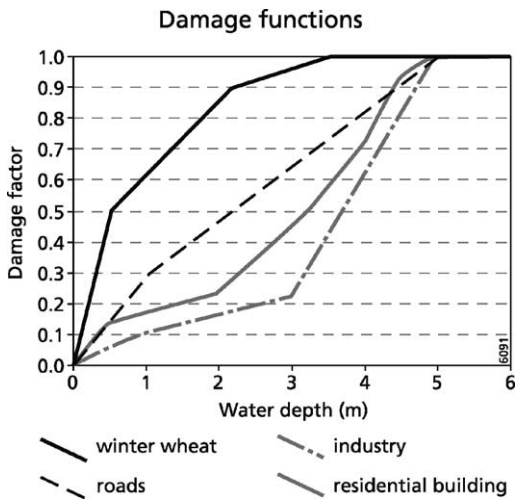

Fig. 5. Damage functions between relative damage and water depth. Source: Vrisou van Eck and Kok (2001); Kok (2001); Staatscourant (1998).

Table 7
Maximum flooding damage values collected from the literature

Land use class	Maximum damage per square meter in 1995 (€)	Source
Winter wheat	0.13	Staatscourant (1998)
Roads	15.74	Vrisou van Eck and Kok (2001)
Industry	68.07	Kok (2001)
Residential	1861.90	Vrisou van Eck and Kok (2001)

- The price level of 1995 was taken as a standard.
- Damage to cars was not considered here as the flood event was announced and the majority of cars were removed before the flood arrived.
- Previous analysis of data of Meuse flooding (Kok, 2001) showed that municipalities which are frequently inundated sustain generally less damage per house than municipalities with less frequent flood events: 'people are less prepared'. This factor was not considered here.
- The variability of average damage per land cover class is considerable. Damage is a function of many physical and behavioral factors. In this study, we used average values of damage estimates.

Fig. 6. Estimated financial damage map based on the IKONOS-2 land cover map. Graduated color map; dark red: high damage rates, light red: low damage rates; white: no damage or no information.

Table 8
Estimated damage values for the IKONOS-2-derived land cover map and computed water depth by the LISFLOOD model

Land use classes in the Borgharen area	Estimated damage (€ × 1000)
(111) Residential building	66625
(112) Private/public garden	1252
(113) Grass in built-up area	0.68
(114) Pavement/other urban area	313
(115) Waterside	80
(141) Road	2650
(143) Railroad	0
(151) Industrial company/agency	314
(211) Pasture	36
(212) Winter wheat	109
(221) Nursery	646
(241) Fallow	0
(331) Natural vegetation	0
(41) Deciduous forest land	0
(43) Mixed forest land	0
(5) Water	0
Total amount of damage (€ × 1000)	72030

Fig. 6 shows the spatial distribution of the estimated property damage in the study area under the assumptions listed above. The most significant damage was sustained in the southern, upstream village of Borgharen. Table 8 shows the estimated damage per thematic land cover class. Residential properties account clearly for the majority of the costs and might ultimately lead to a resettlement of the villages beyond the floodplain. Although the damage estimates seem fairly reliable, the obtained accuracy is a function of the reliability of the available damage functions discussed previously, the estimated price level, the computed water depth in the model and the accuracy of the land cover derived from IKONOS-2. The presented method to calculate flood damage is fast, straightforward and easy to implement for local or regional governments and insurance companies.

5. Conclusions and recommendations

Flooding is a major environmental threat as may be proven by the many flooding events worldwide over the last 10 years. Earth observation techniques may contribute significantly to improve our efforts to model flood events, to develop proper mitigation strategies

and to assess damage to residential properties, infrastructure and agricultural crops. Detailed and reliable land cover maps are required for these applications. The new generation of high spatial resolution satellite sensors such as those aboard IKONOS-2 are suitable instruments to provide that information. In this article we presented a methodology to analyze IKONOS-2 data by combining the use of spectral, spatial and contextual information captured by the image to produce an accurate land cover map. Overall accuracy of the classification is 74%. In spite of the good results of land cover mapping a number of classes such as residential areas and roads are still fairly difficult to identify.

The IKONOS-2-derived land cover map proved a valuable tool to integrate with flood simulation models to produce detailed Manning roughness factor maps of the inundated areas and to simulate flow velocity. IKONOS-2-derived maps are more accurate for flood simulations and property damage assessment than the maps derived from datasets such as the EU CORINE land cover map. An indicative map presenting the estimated damage for 1995 flood event was produced for the Itteren and Borgharen region on the basis of land cover, water depth extracted from the LISFLOOD model and by known relations between water depth and property damage. Such a map is useful information for decision makers and insurance companies.

Acknowledgements

We gratefully acknowledge Rijkswaterstaat Directie Limburg (Maastricht, The Netherlands), Dienst Hydrologisch Onderzoek (Brussels, Belgium), and RIZA (Arnhem, The Netherlands) for their cooperation and for making various datasets available for this study.

References

Anderson, J.R., Hardy, E.E., Roach, J.T., 1976. A land use and land cover classification system for use with remote sensor data. Geological survey professional paper 964. US Government Printing Office, Washington, DC.

Baatz, M., Schäpe, A., 2000. Multi-resolution Segmentation: an optimisation approach for high quality multi-scale image segmentation. AGIT 2000. In: Strobl, J., Blaschke, T., Griesebner, G. (Eds.), Proceedings of the Angewandte Geographische Informationsverarbeitung XII Beiträge Zum AGIT-Symposium Salzburg 2000, pp. 12–23.

Ballard, A., Brown, C.M., 1982. Computer Vision. Prentice-Hall Inc., Englewood Cliffs, NJ, 523 pp.

Bates, P., De Roo, A.P.J., 2000. A simple raster-based model for flood inundation simulation. J. Hydrol. 236, 54–77.

Beasley, D.B., Huggins, L.F., 1982. Answers Users Manual. UESPA, Region V, Chicago, IL, Purdue University, West Lafayette, IN, 54 pp.

Blaschke, T., Strobl, J., 2002. What's wrong with pixels? Some recent developments interfacing remote sensing and GIS. GeoBIT/GIS: J. Spatial Inform. Decision Making, No. 6/2001, pp. 12–17.

Chow, V.T., 1959. Open-Channel Hydraulics, ISBN 0-07-010810-2. McGraw-Hill, New York, 572 pp.

De Jong, S.M., Bagré, A., Van Teeffelen, P.B.M., Van Deursen, W.P.A., 2000. Monitoring trends in urban growth and surveying city quarters in the city of ouagadougou, burkina faso using SPOT-XS. Geo. Int. 15 (2), 61–68.

De Roo, A.P.J., 1999. LISFLOOD: a rainfall-runoff model for large river basins to assess the influence of land use changes on flood risk. In: Balabanis, P. et al. (Eds.), Ribamod: River Basin Modelling, Management and Flood Mitigation. Concerted Action, European Commission, EUR 18287 EN, pp. 349–357.

De Roo, A.P.J., Price, D.A., Schmuck, G., 1999a. Simulating the Meuse and Oder floods using the LISFLOOD model. In: Fohrer, N., Doell, P. (Eds.), Proceedings of the Giessen Meeting on Modellierung des Wasser-und Stofftransports in Grossen Einzugsgebieten, Kassel University Press, Kassel, 12–14 November 1998, pp. 41–50.

De Roo, A.P.J., Van Der Knijff, J., Horritt, M., Schmuck, G., De Jong, S.M., 1999b. Assessing flood damages of the 1997 Oder flood and the 1995 Meuse flood. In: Proceedings of the Second International ITC Symposium on Operationalization of Remote Sensing, Enschede. The Netherlands, 16–20 August 1999, 8 pp (Published on CD-ROM).

De Roo, A.P.J., Wesseling, C.G., Van Deursen, W.P.A., 2000. Physically based river basin modelling within a GIS: the LISFLOOD model. Hydrol. Processes 14, 1981–1992.

eCognition, 2002. User Guide. Definiens Imaging GmbH, Munich, 65 pp. Available via website: http://www.definiens-imaging.com/product.htm (December 2002).

HAZUS, 2001. Hazus Flood Loss Estimation Model. Available on Internet site: http://nibs.org/hazusweb (December 2002).

Hofmann, P., 2001. Detecting Buildings and Roads from IKONOS-2 Data Using Additional Elevation Information. GeoBIT/GIS: J. Spatial Infor. Decision Making, No. 6/2001, pp. 28–33.

Janssen, L.L.F., 1994. Methodology for Updating Terrain Object Data from Remote Sensing Data. Ph.D. Thesis. Landbouw Universiteit Wageningen, Wageningen, The Netherlands.

Jensen, J.R., Cowen, D.C., 1999. Remote sensing of urban/sub-urban infrastructure and socio-economic attributes. Photogram. Eng. Remote Sens. 65 (5), 611–622.

Kok, M., 2001. Stage-Damage functions for the Meuse River Floodplain. Communication Paper to the Joint Research Centre, Ispra, Italy, 10 pp.

Lillesand, T.M., Kiefer, R.W., 2000. Remote Sensing and Digital Image Interpretation. Wiley, New York, 724 pp.

Limp, W.F., 2002. Quick-Take Review of eCognition. Geoworld No. 0204, pp. 53–54.

Penning-Rowsell, E., 2001. Stage-Damage Functions for Natural Hazards Unit. Flood Hazard Research Centre, Middlesex University, England. Communication Paper to the Joint Research Centre, Ispra, Italy, 3 pp.

Penning-Rowsell, E., Fordham, M., 1994. Floods Across Europe. Hazard Assessment, Modelling and Management. ISBN 1 898253 01 3. Middlesex University Press, Middlesex, 214 pp.

Roberts, L.G., 1970. Machine Perception of Three Dimensional Solids. In: J.T. Tippett, D.A. Berkowitz, L.C. Clapp (Eds.), Optical and Electro-Optical Image Processing, MIT Press, Cambridge, MA, pp. 159–197.

Richards, J.A., 1999. Remote Sensing and Digital Image Analysis: An Introduction, 2nd ed. Springer, Berlin, Heidelberg, 363 pp.

Schoenmakers, R.P.H.M., 1995. Integrated Methodology for Segmentation of Large Optical Images in Land Applications of Remote Sensing. Ph.D. Thesis. Nijmegen University. Institute for Remote Sensing Applications, Joint Research Centre, European Commission, I-21020, Ispra, Varese, Italy.

Staatscourant, 1998. Regeling oogstschade 1998. Staatscourant 1998, no. 244. Ministerie van Algemene Zaken, Den Haag, pp. 16–17.

Thunnissen, H.A.M., De Wit, A.J.W., 2000. The national land cover database of The Netherlands. In: Beek, K.J., Molenaar, M. (Eds.), Proceedings of the XIX Congress of the International Society for Photogrammetry and Remote Sensing (ISPRS) Geoinformation For All. Lemmer, GITC, 2000. Int. Arch. Photogramm. Remote Sens. 33 (Part B7/3), 223–230 (CD-ROM).

Tilton, J.C., 1989. Image segmentation by iterative parallel region growing and splitting. In: Proceedings of the International Geoscience and Remote Sensing Symposium (IGARSS). Vancouver, Canada, pp. 2235–2238.

Vrisou van Eck, N., Kok, M., 2001. Standaardmethode Schade en Slachtoffers als gevolg van overstromingen. Dienst Weg-en Waterbouwkunde. Ministerie van Rijkswaterstaat, The Netherlands. Publicatie-no. W-DWW-2001-028, April 2001, 38 pp.

White, G.F., 1945. Human Adjustments to Floods: A Geographical Approach to the Flood Problem in the United States Doctoral Dissertation and Research paper no. 29. Department of Geography, University of Chicago.

Wilson, R., Spann, M., 1988. Image Segmentation and Uncertainty. ISBN: 0-86380-067-X. Research Studies Press, Letchworth, 180 pp.